

# Current status of the LEPS2 Solenoid Spectrometer

LEPS2 collaboration

March 31, 2024

## 1 Overview

(M. Niyama)

The LEPS2 experiment at SPring-8 has been built for hadron photoproduction experiments using linearly-polarized photon beams with energies of 1.5-3 GeV. The LEPS2 detector is shown schematically in Fig. 1. The detector covers polar angles of charged particles between  $10^\circ$  and  $120^\circ$  arising from reactions in the cryogenic target at the center of the detector. Also, the Barrel  $\gamma$  Counter ( $B\gamma$ ) covers polar angles of photons between  $40^\circ$  and  $110^\circ$ .

The core of the LEPS2 spectrometer is a solenoid with a bore diameter and overall yoke length of approximately 3 m and 3.5 m, respectively. This solenoidal magnet previously used for the kaon rare-decay experiment at BNL-AGS, E787/E949 [1], and was shipped from the Brookhaven National Laboratory, New York to SPring-8, Hyogo, Japan in 2011. The target is located inside the upstream bore of the magnet.

The spectrometer consists of the Start Counter (SC), the Time Projection Chamber (TPC), the Drift Chamber (DC), the Barrel Resistive Plate Chamber (BRPC), the Forward Resistive Plate Chamber (FRPC), the Barrel  $\gamma$  Counter ( $B\gamma$ ), the Neutron Counter (NC), and the Aerogel Cherenkov Counter (AC). Figure 1 schematically depicts the solenoid spectrometer. The solenoid magnet, operated at 0.9 T, allows us to perform momentum analysis of the charged particles. A liquid hydrogen, deuterium, or nuclear target can be installed inside the TPC. The DC and the TPC detect charged particles scattered at forward angles and sideways, respectively. The SC, located close to the target, measure the timing of charged particle production using RF information from the electron storage ring. FRPC detect charged particles scattered at forward angles approximately 4 meters downstream from the target, and BRPC detect charged particles in large scattering angle regions at a radial distance of 0.9 meters. FRPC and BRPC provide time-of-flight (TOF) information of charged particles with a resolution around 100 ps. The particle mass is determined from the momentum and velocity of a charged particle. For high-momentum pions, AC are used for identification. In addition to charged particles, photons and neutrons are detected using  $B\gamma$  and NC, respectively.

### 1.1 Momentum resolution

(R. Kobayakawa and M. Niyama)

The spectrometer was originally designed to study excited hyperons and an exotic penta-quark candidate. The target position was optimized to measure kaons and pions in the polar angular range from 10 to 110 degrees.

The trajectories of charged particles scattered at forward angles are measured with four packages of the DC, and those scattered sideways are measured with the TPC. To reduce multiple scattering for forward-going particles, the downstream end of the TPC is made of thin membranes. The length of the TPC was optimized to measure particles from 40 to 110 degrees, and its radius was determined so that the momentum resolution from position measurement was comparable to that from multiple scattering. Fig. 2 shows the expected momentum resolution for 1 GeV/c kaons as a function of the scattering angle. Particles scattered at forward polar angles ( $10 \sim 20^\circ$ ) are measured with the DC. Conversely, particles at large scattering angles ( $40 \sim 120^\circ$ ) are measured with the TPC. In the polar angular range of  $20 < \theta < 35^\circ$ , both DC and TPC are employed for tracking.

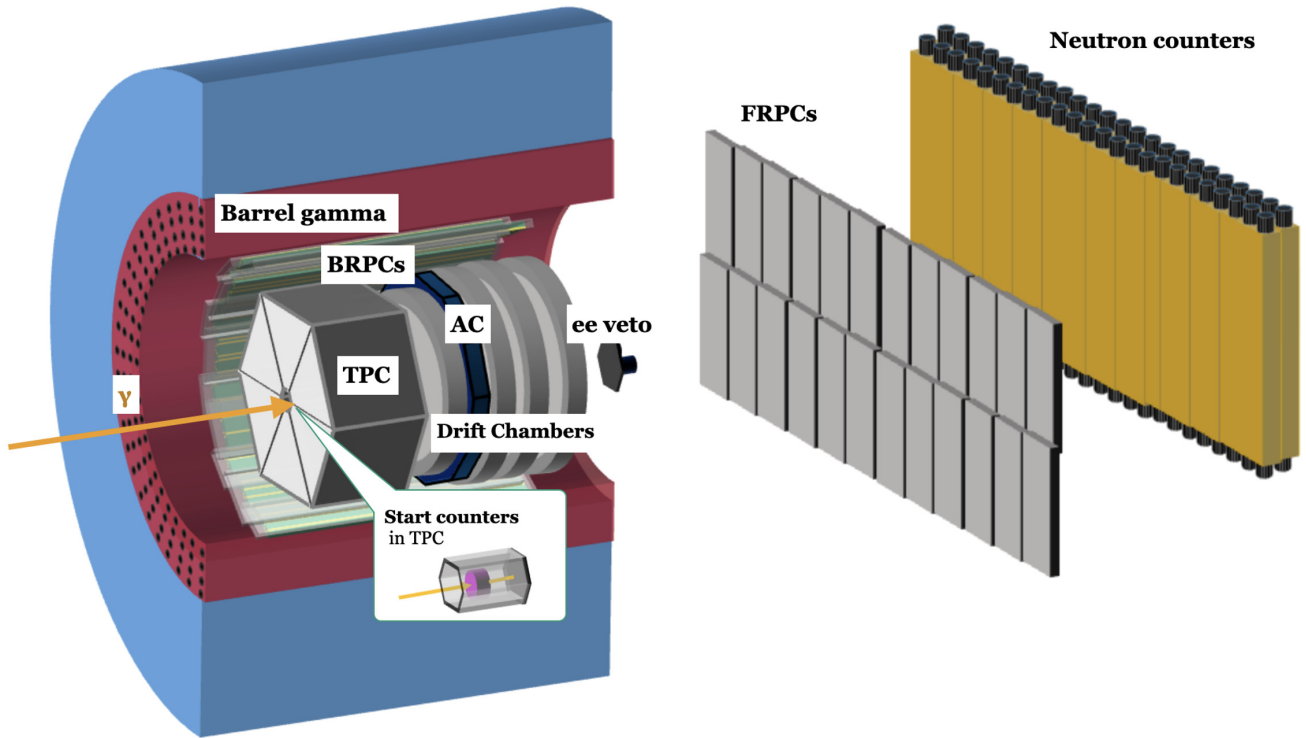


Figure 1: Schematic view of the LEPS2 solenoid spectrometer.

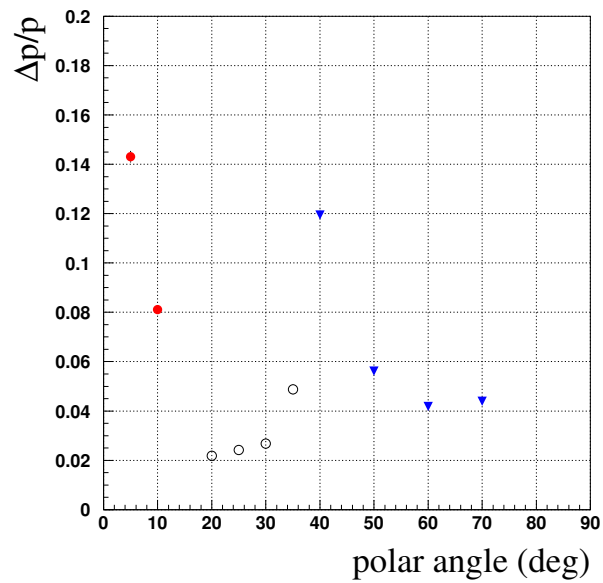


Figure 2: Expected momentum resolutions for 1 GeV/c kaons detected by DC, TPC, and both of DC and TPC are shown as blue triangle, red open circles, black open circles, respectively.

## 1.2 Particle identification

(R. Kobayakawa)

### 1.2.1 Particle identification using TOF and momentum measurements

Particle identification, especially for kaons, is crucial for studying hadron production with strangeness. We use TOF,  $dE/dx$  in the TPC, and Cherenkov counters for this purpose. When an excited hyperon is produced at LEPS2, via  $\gamma N \rightarrow K^+ Y^*$  reactions, the maximum momentum of kaons scattered in the forward region is about 1.4 GeV/c. These kaons can be distinguished from pions with a separation power of  $3.5\sigma$  using a 120 ps TOF resolution and approximately 4 m flight length. Aerogel Cherenkov counters assist in identifying high-momentum kaons from pions. In the large polar angle regions, low-momentum particles less than 1 GeV/c are scattered. To identify them using TOF, we employed the BRPC to achieve good timing resolution.

The masses of charged particles are reconstructed using the momenta and TOF measured with the TPC and BRPC, respectively. Figure 3 shows the reconstructed mass with the TPC and BRPC (right), and the separation power (left). The separation power is defined as

$$S_{AB} = \frac{|O_A - O_B|}{\sqrt{\sigma_A^2 + \sigma_B^2}} \quad (1)$$

where  $O_{A(B)}$  is the reconstructed mass value of particle A(B) and  $\sigma_{A(B)}$  is the mass resolution of particle A(B). Particles with momentum less than approximately 0.4 GeV/c are identified using  $dE/dx$  versus momentum correlations measured with the TPC, as shown in section 2.5.

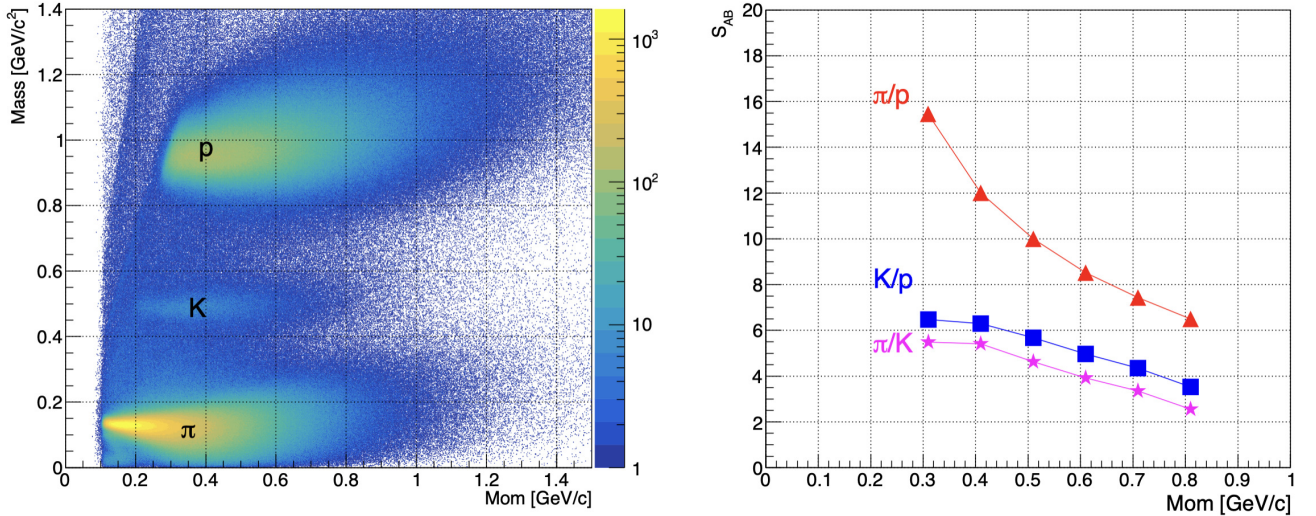


Figure 3: Particle Identification with the TPC and BRPC

### 1.2.2 Particle identification using $dE/dx$

Particle identification in the side region is performed by combining the energy loss value ( $dE/dx$ ) and the reconstructed momentum value measured by the TPC. The pulse height of the TPC signal provides a value corresponding to the energy loss ( $dE$ ). The  $dE/dx$  of a given track is obtained by taking the truncated mean of  $dE$  of hits and dividing it by the track's path length on the readout pad. Figure 4 shows the TPC  $dE/dx$  versus reconstructed momentum (left), and  $\pi/proton$  separation power with TPC  $dE/dx$  (right). The track required more than 15 hits in the TPC.

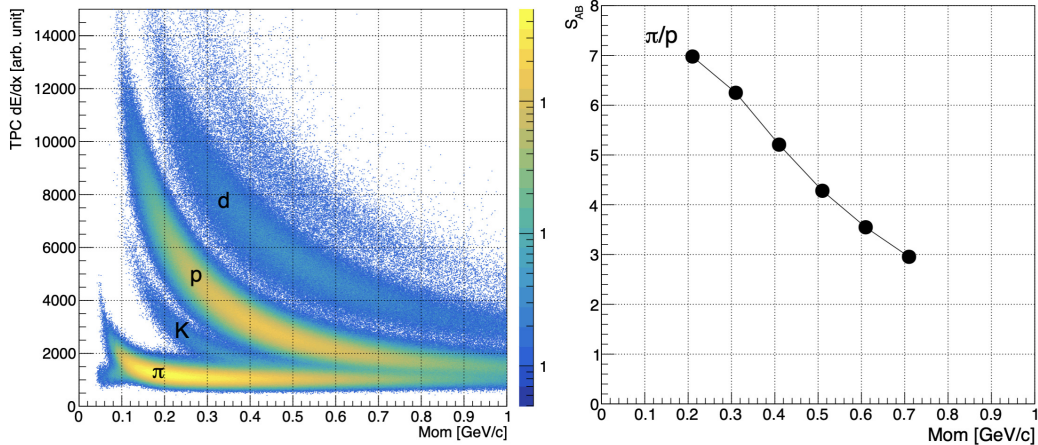


Figure 4: Particle Identification using TPC  $dE/dx$

### 1.3 Event rate and data acquisition system

The total hadronic cross sections of  $\gamma d$  collisions in our energy range are 0.26 to 0.3 mb, and the event rate of hadron production is estimated to be approximately 300 cps when 1 Mcps photons are irradiated onto the 15 cm liquid deuterium target. We aim to accumulate hadron production events with minimal selection bias. For the data acquisition trigger, we require signals from the tagging counters (TAG) and start counters (SC). Electrons and positrons in the photon beam are eliminated using a plastic scintillator (UP counter) at the trigger level.  $e^+e^-$  pair production events in the target are also eliminated using a plastic counter (EE counter) located downstream of DC4. The number of SC hits is adjusted to optimize data acquisition efficiency. For liquid hydrogen target runs, we require at least one hit in the side slats of the SC, and for liquid deuterium target runs, at least two hits. The typical trigger rates are about 100 cps for both cases, with a tagging photon counter rate of approximately 1 Mcps.

## 2 Description of each detector

### 2.1 Start Counter (SC)

(M. Yosoi)

The Start Counter(SC) is a trigger detector covering a large solid angle that detects charged particles and outputs a start timing signal for the data acquisition system when a photo-produced reaction occurs at the target. The following characteristics are required for SC;

- 1) quick response to produce the trigger signal,
- 2) better timing resolution than 300 ps for selecting the proper beam bunch among the RF bunches of 2 ns interval,
- 3) operational in the high magnetic field (nearly 1 T),
- 4) identify multiple event with more than one charged particle.

To satisfy these requirements, a segmented scintillation counter using MPPCs for light signal read out has been employed as SC.

#### 2.1.1 Mechanical design

SC is composed of two parts, Fwd-SC (FSC) and Side-SC (SSC) as shown in Fig. 5. Each plastic scintillator is ELJEN EJ-212 with the thickness of 4 mm and HAMAMATSU MPPC S13360-3050PE are used to read out the light signal.

FSC is placed downstream of the target and detect charged particles emitted forward. It has a hexagonal shape consisting of four pieces of trapezoidal scintillators. Six MPPCs are attached to each

side of each trapezoidal scintillator via a thin (1 mm thick) UV filter light guides. (UV filter is inserted to reduce the Cherenkov components in the light.) Each scintillator is separated from its neighbors by only very thin aluminized mylar films, and after making the hexagon, FSC is covered a black sheet. Then, there is almost no insensitive area.

SSC consists of six rectangular scintillators, forming a hexagonal cell structure. Charged particles emitted in the lateral direction are detected by SSC. Eight MPPCs are attached to each end of each scintillator via a thin UV filter light guide, as in the FSC.

FSC is attached to the downstream end of the SSC. Whole SC is inserted into a thin Kapton cylinder holder and then installed in the inner bore of TPC.

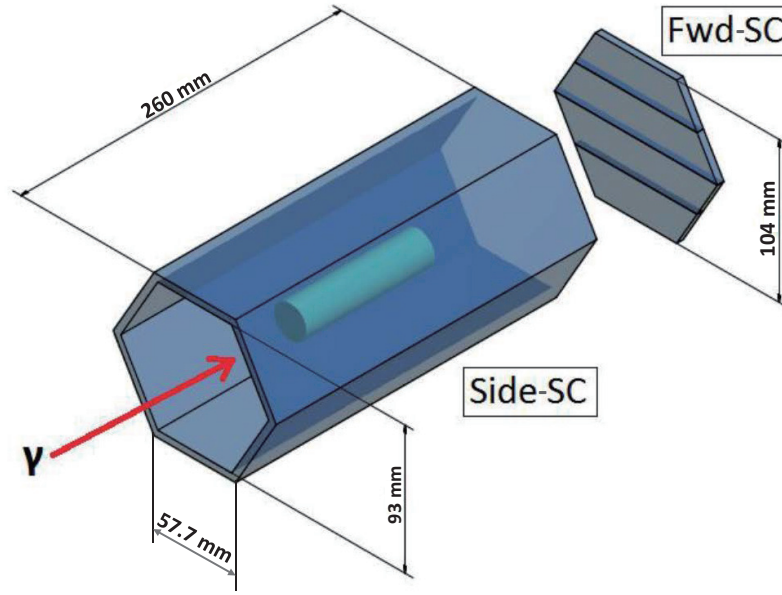


Figure 5: Schematic view of the Start Counter (SC).

### 2.1.2 Performance study

Before installing SC in the LEPS2 solenoid-spectrometer system, each scintillator of SC was tested for performance evaluation using a positron beam at the LEPS beamline. As a result, we confirmed that all scintillators achieved a time resolution of less than 150 ps, and that the dependence of the resolution on the irradiation position of each scintillator was very small. (Here, the time resolution was evaluated by the  $\sigma$  of the distribution of  $T_{diff} = T_{mean} - T_{RF}$ , where  $T_{mean}$  is the average time of the signals from MPPCs at both ends after slewing correction for differences in pulse height and  $T_{RF}$  is the time of the RF signal from the SPring-8 accelerator.)

In the LEPS2 experiments, a long liquid hydrogen or deuterium target of about 15 cm is used. In this case, the reaction time depends on the reaction point of the target, and the arrival time of the emitted particle to each scintillator depends on the velocity and direction. Then, the distribution of  $T_{diff}$  of each scintillator becomes broad and asymmetric, and tails toward the slow side, resulting in a time resolution of about 300 ps, which is just barely enough to distinguish RF bunches at 2 ns intervals. However, it is rare for a slow charged particle to be emitted alone, and in most cases the faster particle is detected by another scintillator at the same time. When such a multi-hit event occurs, by selecting the scintillator that  $|T_{diff} - T_{diff}^{peak}|$  is minimum, where  $T_{diff}^{peak}$  is the most probable value of  $T_{diff}$  distribution, the time resolution of the  $T_{diff}(min)$  distribution becomes less than 120 ps for multi-hit events as shown in Fig. 6. Even including single-hit events, the resolution is less than 160 ps with this method, which is sufficient for RF bunch selection.

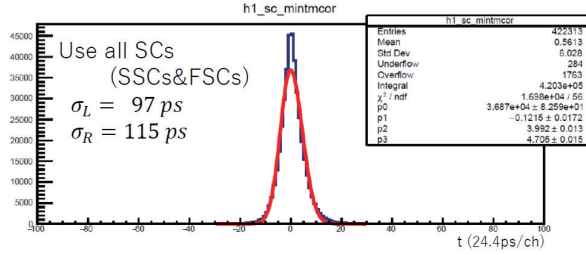


Figure 6: Time resolution of SC for multi-hit events when using 15 cm long liquid deuterium target

## 2.2 Aerogel Čerenkov Counter (AC)

(A.O. Tokiyasu)

### 2.2.1 Mechanical design

The Aerogel Cherenkov Counter (AC) is composed of 36 modules each consisting of aerogel acting as a radiator and a Photomultiplier Tube (PMT) for detecting Cherenkov light.

The configuration of each module is shown in Fig.2.2.1-(a). The aerogel has a refractive index of 1.03 and a thickness of 60mm. The AC operates as a threshold-type particle identification, capable of distinguishing between  $\pi$  and  $K$  mesons up to a maximum momentum of 2.0 GeV/ $c$ . Each module is trapezoidal in shape, with dimensions of 258mm in height, 146mm for the longer side, and 92mm for the shorter side. The aerogel is housed within a black box made of 0.5mm thick polypropylene resin, put on the inside with aluminized Mylar as a reflective material. The black box employs a total-reflection design, optimized with an optical simulation to guide Cherenkov light to the PMT through a light guide most efficiently. Due to the necessity of operating within a magnetic field, a 3-inch FineMesh-type PMT (PMTR5065MOD) was selected. To maximize gain, it is mounted at a 30-degree angle relative to the magnetic field.

Figure 2.2.1-(b) presents a schematic of the assembly of the 36 segments. The system is installed between the DC0 and DC1 to cover the forward angle of 30–40 degrees from the target. In combination with the tracking information from the TPC and the RPC, it performs particle identification for  $\pi$  and  $K$  mesons. Currently, 35 segments are installed between DC0 and DC1 (Fig.2.2.1-(c)), and physics data acquisition is underway. Charge information is collected using a CAEN-V792, while time information is obtained with a CAEN-V1190A.

### 2.2.2 Performance study

Before installation, we conducted a performance evaluation of the modules using a 600 MeV/ $c$   $e^+$  beam at ELPH, Tohoku University. Trigger scintillators of 10mm size were installed upstream and downstream of the module. By using the trigger information, we derived the module's detection efficiency and the probability of misidentification (misID). Here, detection efficiency and misidentification are defined as follows:

$$\begin{aligned}
 \text{efficiency}(w/\text{aerogel}) &= \frac{\text{Counts}(ADCch > \text{threshold})}{\text{Counts}(Trigger)} \\
 \text{misID}(w/o\text{aerogel}) &= \frac{\text{Counts}(ADCch > \text{threshold})}{\text{Counts}(Trigger)}
 \end{aligned}$$

We also investigated the dependency on the position of irradiation on the module. The results are shown in Fig.8. The position marked '0' indicates the location furthest from the PMT.

misidentification refers to the probability of detecting a signal with the box alone, without the aerogel. It was found that closer to '0', the detection efficiency decreases down to 80%, but at distances greater than 50mm, a detection efficiency of over 95% was achieved.

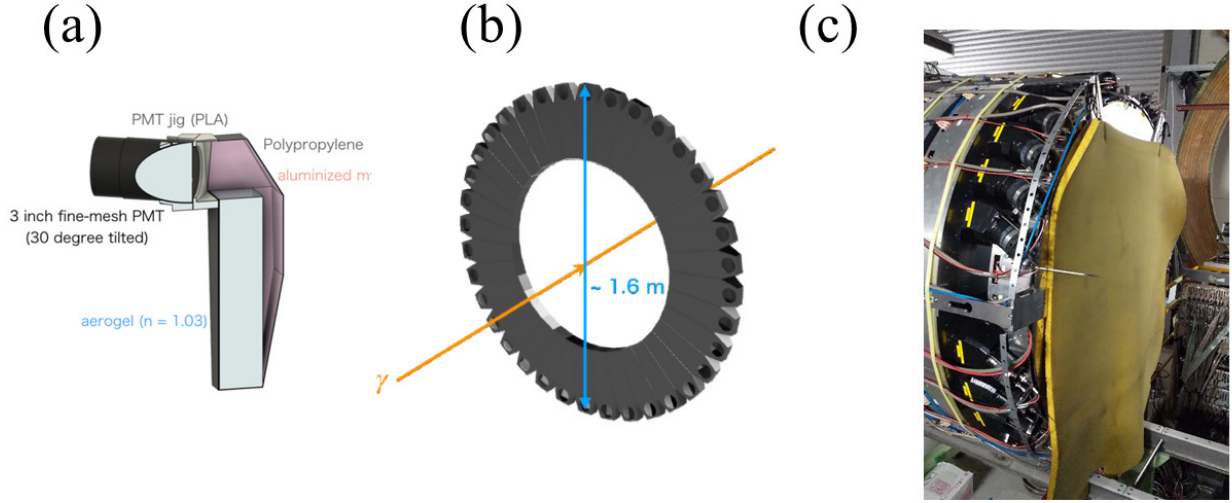


Figure 7: LEPS2 AC configuration: (a) schematic view of one module (b) schematic view of combined 36 modules (c) photos of installed AC.

## 2.3 Resistive Plate Chamber (RPC)

(M. Niiyama)

For the time-of-flight measurement of charged particles, we employ FRPC in the forward polar angle region and BRPC in the large polar angle region. The number of gaps and stacks of FRPC and BRPC are the same, but the lengths of the readout strips are different. The time resolutions of both RPC were about  $\sim 100$  ps.

For both of FRPC and BRPC, a five gap, double-stack configuration is adopted. The readout strips of FRPC and BRPC are  $\sim 2.5 \times 100 \text{ cm}^2$  and  $\sim 2.5 \times 200 \text{ cm}^2$ , respectively. These large readout strips allow us to cover large area with the small channel numbers of readout electronics. The details of the mechanical design can be found in elsewhere [3, 4]. The FRPC are located about 4 m downstream from the target, and the BRPC are at a radial distance of 0.9 m from the target. The timing resolution were around 100 ps for both RPC. Figure 9 shows the time resolution of BRPC as a function of the hit position of electrons in the RPC, where zero of x-axis is the center of the RPC. The start timing is determined with resolution better than 20 ps utilizing the RF signal of the SPring-8 storage ring. Thus, the time-of-flight resolutions are dominated by the time resolution of RPC.

## 2.4 Drift Chambers (DC)

(M. Niiyama)

### 2.4.1 Mechanical design

The charged particles scattered at forward angles are detected using four drift chambers, DC0 to DC3. Each DC is of the planar type and contains 6 wire planes with three wire directions,  $90^\circ$  (Y),  $30^\circ$  (U), and  $-30^\circ$  (V) in the azimuthal angles. Two planes with the same directions are shifted by half the

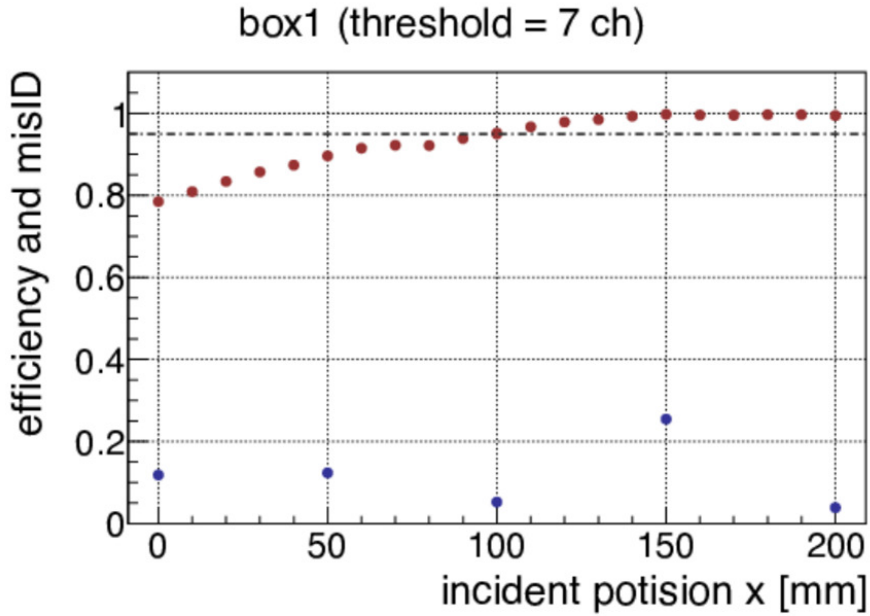


Figure 8: The incident position dependence of efficiency (red dot) and misID (blue dot) of AC.

length of the wire pitch. The effective areas of each plane are hexagonal in shape, and the diameters of the inscribed circles are 1024 mm and 1280 mm for DC0 and the others, respectively. Since DC0 is closer to the target, its radius is smaller than that of the others. Each plane is separated by a cathode plane, and the wire pitch is 8 mm, as shown in Fig. 10. The gas mixture used were 50% argon and 50% ethane.

#### 2.4.2 Performance study

The efficiency and position resolution of DC1 were studied using an  $e^+$  beam in LEPS1. Data were collected at various incident particle angles for DC1. The gas mixture used in this DC consists of 70% argon and 30% isobutane. With appropriate voltages, the efficiency is more than 99% in all planes. Fig. 11 shows the voltage dependence of efficiency for each plane. The position resolution is approximately 150  $\mu\text{m}$ . Figs. 12, 13, and 14 show the angle dependence of position resolution in each plane. There is a tendency for the position resolution to improve as the particle angle increases.

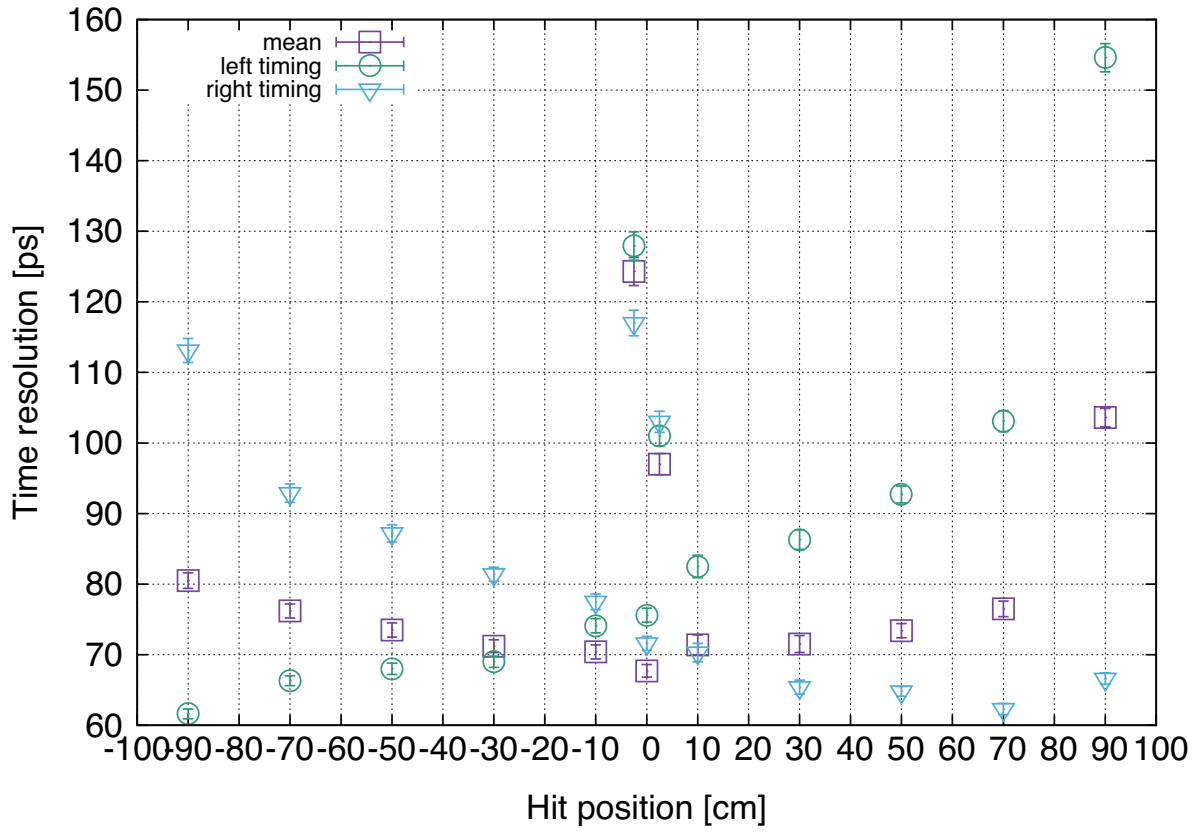


Figure 9: Time resolution as a function of the hit position of RPC.



Figure 10: The wire geometry of the drift chamber

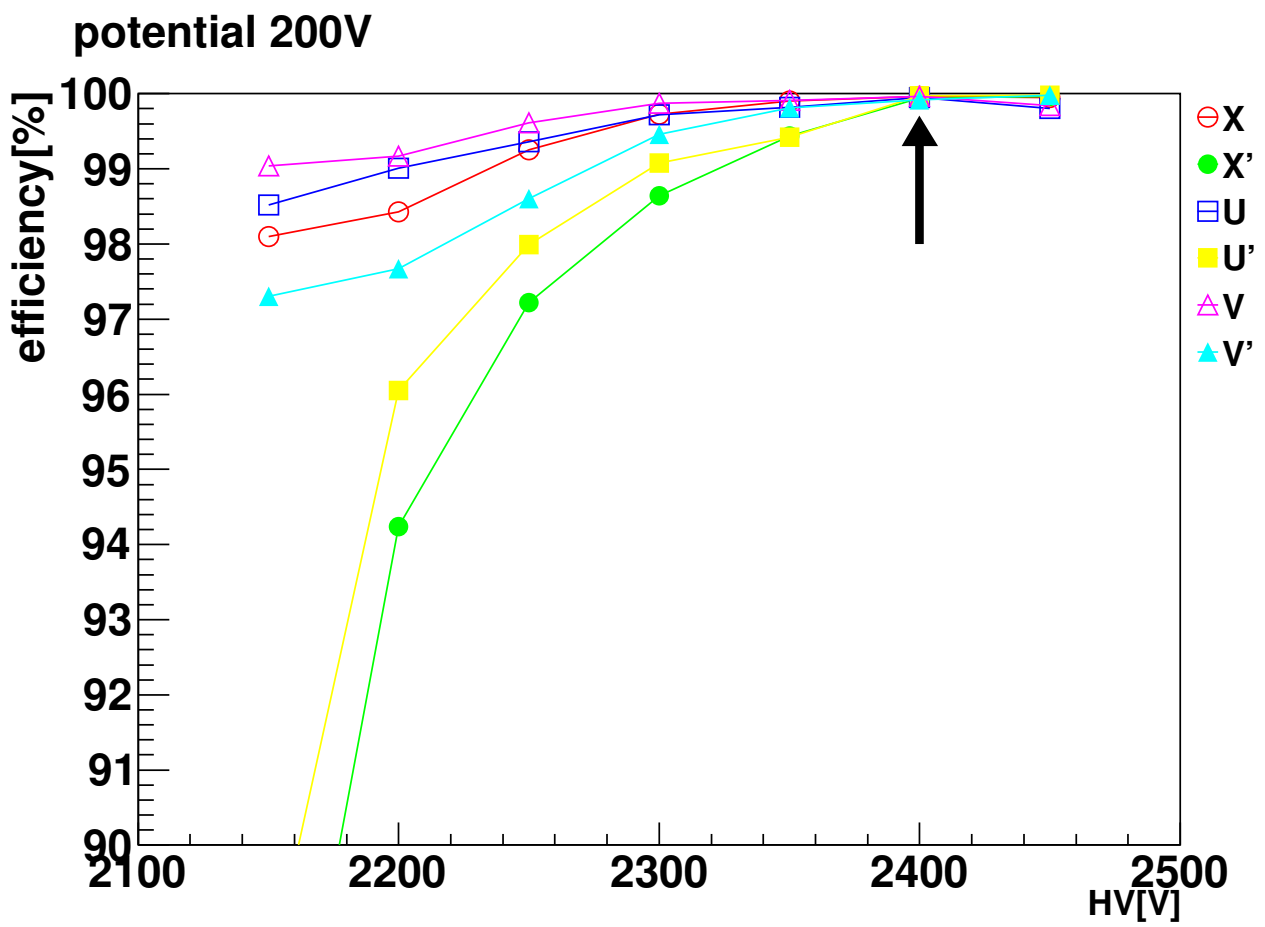


Figure 11: The voltage dependence of efficiencies in each plane of DC

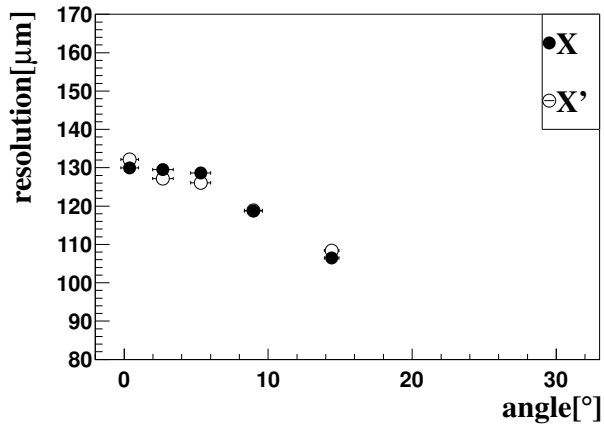


Figure 12: The angle dependence of position resolution in X and X' planes

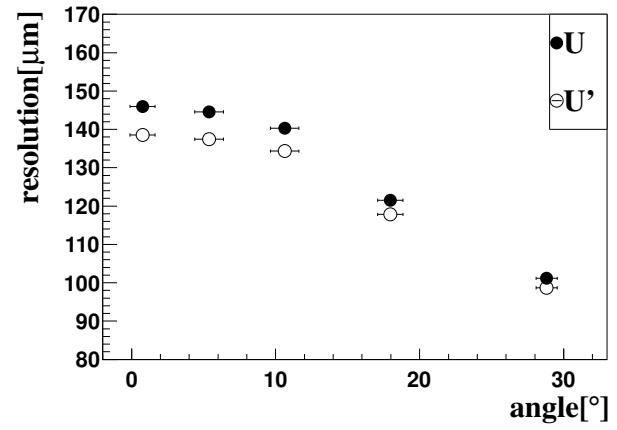


Figure 13: The angle dependence of position resolution in U and U' planes

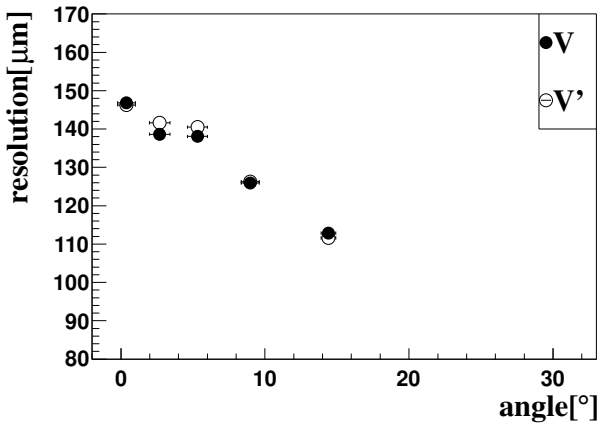


Figure 14: The angle dependence of position resolution in V and V' planes

## 2.5 Time Projection Chamber (TPC)

### 2.5.1 Mechanical design

The TPC has a hexagonal shape with a drift length of 710 mm and an active radius of 655 mm. The target is installed inside of the TPC and particles scattered at 40-120 degrees are measured. Fig. 15 shows the schematic view of the readout plane of the TPC, where readout pads are drawn in the one sector. Table 1 shows the specification of the TPC.

The spatial resolution of the TPC is typically 0.4 mm and 0.8 mm.  $r\phi$  and  $z$  (drift direction), respectively.

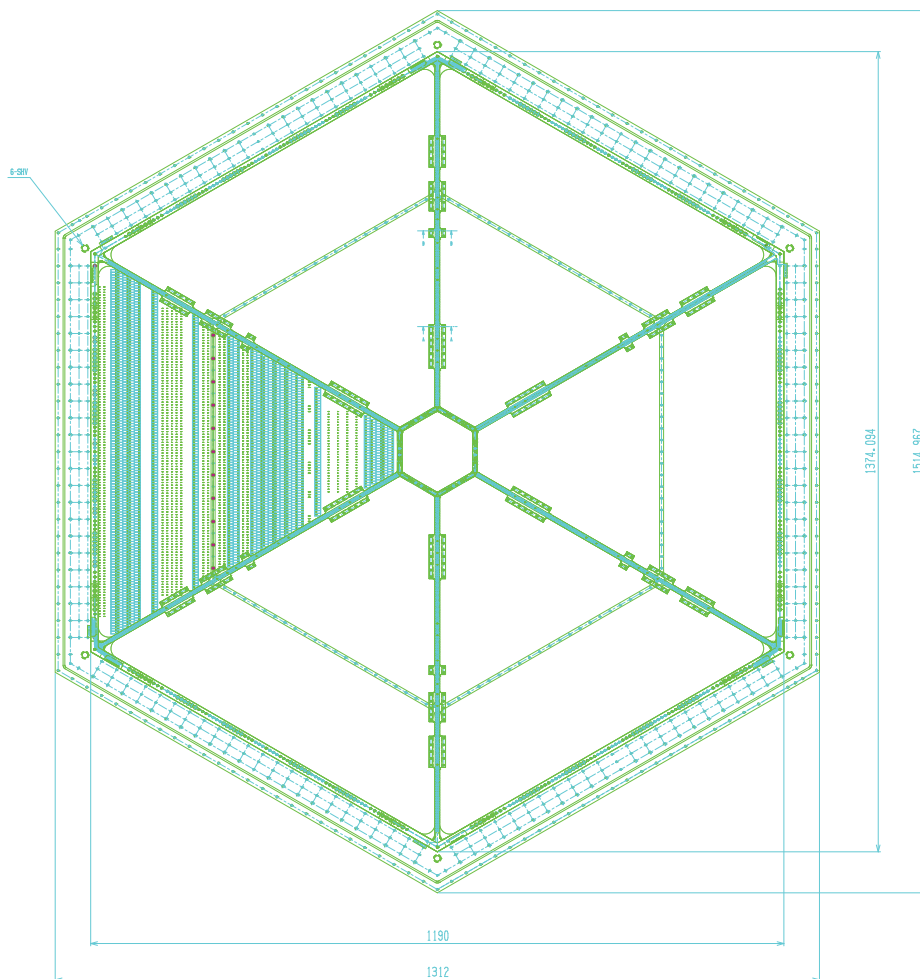


Figure 15: Design view of the readout plane of the TPC.

### 2.5.2 TPC Performance

Various factors contribute to the spatial resolution of the LEPS2TPC. The following formula expresses the resolution in the  $r\phi$  and  $z$  directions.

$$\sigma_{r\phi}^2 = \sigma_{r\phi,int}^2 + \frac{dE_{MIP}}{dE} \{ \sigma_{r\phi,0}^2 + \sigma_{r\phi,D}^2 L_D + \sigma_{P,W}^2 \tan^2 \theta \} \quad (2)$$

$$\sigma_z^2 = \sigma_{z,int}^2 + \frac{dE_{MIP}}{dE} \{ \sigma_{z,0}^2 + \sigma_{z,D}^2 L_D + \sigma_{dip}^2 \tan^2 \lambda \} \quad (3)$$

We estimated the dependence of each factor using cosmic ray and beam data. Table 2 shows the parameters of spatial resolution for Track Fitting.

Table 1: Specification of the TPC

Spatial resolution in $r\phi$ (drift direction)	0.4 mm (0.8 mm)
Drift length	710 mm
The radius of effective area	655 mm
Number of pads	10830
pad size	$4.6 \times 10 \text{ mm}^2$
Number of anode (potential) wires	99 (100)
Diameter of anode (potential) wire	25 (80) $\mu\text{m}$
Material of anode (potential) wire	Au-W (Au-BeCu)
Gas type	P10

Table 2: The parameter of the spatial resolution

$r\phi$ -direction	parameter value	$z$ -direction	parameter value
$\sigma_{r\phi,int}$ [mm]	0.129	$\sigma_{z,int}$ [mm]	0.377
$\sigma_{r\phi,0}$ [mm]	0.223	$\sigma_{z,0}$ [mm]	0.447
$\sigma_{r\phi,D}^2$ [mm]	0.000398	$\sigma_{z,D}^2$ [mm]	0.00196
$\sigma_{P,W}$ [mm]	1.26	$\sigma_{dip}$ [mm]	1.51

## 2.6 Barrel Gamma Detector ( $B\gamma$ )

(M. Sumihama)

The Barrel Gamma Detector ( $B\gamma$ ) is a sampling calorimeter. The  $B\gamma$  is placed most outside of the detector system at a distance of 1 m from the target. The  $B\gamma$  detects  $\gamma$  rays from the decay of  $\pi^0$ ,  $\eta$ ,  $\Sigma^0$  hyperon, and so on. The particle identification is performed by Energy deposition which is determined by summing up the signals of each module. The energy of gamma-rays from  $\pi^0$  is expected to be from 200 MeV to 600 MeV with the LEPS2 photon beam. A  $z$ -hit position is determined from the time difference between PMTs on both sides.

### 2.6.1 Mechanical design

As shown in Fig.16,  $B\gamma$  is composed of 48 modules in azimuthal direction and 4 modules in radial direction totalling 192 modules. The size of each module is  $100\sim 130 \text{ mm} \times 140\sim 180 \text{ mm} \times 1.90 \text{ m}$ . The 1.90 m length in the beam direction which corresponds to the geometrical acceptance of 40 – 110 degree from the target center.

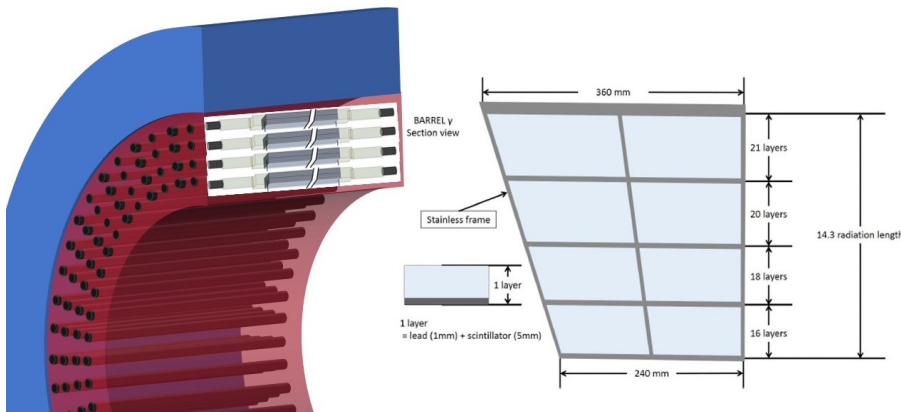


Figure 16: Schematic view of the installation of modules (left) and the layer coordinate (right).

The schematic view of each module is shown in Fig.17. Each module is constructed with a sandwich

structure of lead and scintillator (BC-408) installing in the 1.5 mm-thick stainless steel box. The lead layer is 1 mm thick, and the scintillator layer is 5 mm thick. Four radial modules contain 16, 18, 20, and 21 sandwich layers, respectively. The total radiation length in the radial direction is 12~16. The light guide consists of three parts: a acrylic mixer box with a thickness of 150 mm, silicone cookie (EJ-560), and 67 mm-diameter  $\times$  850 mm-long UVT acrylic light-pipe. The scintillator-lead modules and the acrylic box, and the light-pipe and the PMT are fixed with optical cement(BC-600). The light-pipe and the acrylic box are contacted through the silicone cookie. The PMTs (EMI 9821KB) with a  $\mu$ -metal shield are mounted on the both ends through the light guides. These are placed in the hole of the end cap of the solenoid. There is a magnetic field inside the holes. The magnetic field in a radial direction at the position of PMTs is 16 gauss at the maximum without the  $\mu$ -metal shield and it is reduced to be less than 0.5 gauss by mounting the shield. The magnetic field in a z-direction does not change much by the shield, and it is about 3 gauss.

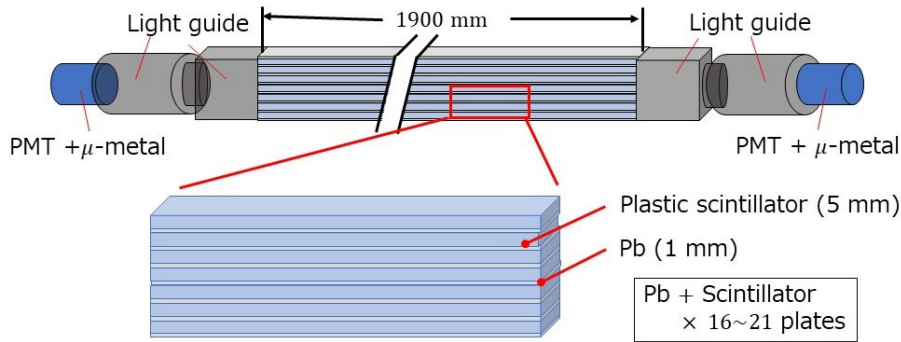


Figure 17: Schematic view of one module of the  $B\gamma$ .

### 2.6.2 Performance study

The performance of  $B\gamma$  was evaluated by using cosmic-ray and positron beam.[5] [6] Cosmic-ray test run was performed from June to September in 2015. Neighboring four modules were used for this test. By measuring the time of flight between each module, we obtained the time resolution of approximately 300 ps for one module. By measuring the relation between the ADC ratio of the PMT's on both side and hit positions of cosmic rays, the attenuation length was obtained to be approximately 1,400 mm. These values are consistent with those measured in the BNL-E787 experiment.

A test experiment was performed using a position beam at ELPH on December in 2015 to check the linearity of the detector response for the deposit energy, and measure the energy resolution. The energy range of the position beam at ELPH was from 50 to 700 MeV. The linearity was checked up to 500 MeV. The energy resolution was found to be approximately 20 MeV for 100 MeV. These values were compared with the Monte Carlo simulation, and were almost consistent.

The gain tuning was performed by using LED lights with the magnetic field. The fine tuning was done by using Cosmic rays that penetrate through the detector from top to bottom with the magnetic field. The minimum ionization peak around 15 MeV was used for the tuning.

The time-walk collection was done with Cosmic rays by a following function,

$$T_{mean} = \frac{TDC_{up} + TDC_{dw}}{2} - \frac{C_1}{ADC_{up}} - \frac{C_2}{ADC_{dw}} - \frac{C_3}{\sqrt{(ADC_{up})}} - \frac{C_4}{\sqrt{(ADC_{dw})}} \quad (4)$$

. Figure 18 shows the scatter plots of  $T_{mean}$  vs. ADC without and with the time-walk collation. The time resolution was determined to be between 340 ps and 550 ps by utilizing cosmic rays that penetrated the detectors vertically. The time resolution does not depend on the z-coordinate.

The beam experiment carried out in 2022. The data was used to determine the attenuation length and the effective velocity of the scintillation lights for each module. Charged particles were selected and these trajectories were obtained by the TPC. The his positions at the  $B\gamma$  were expected by the

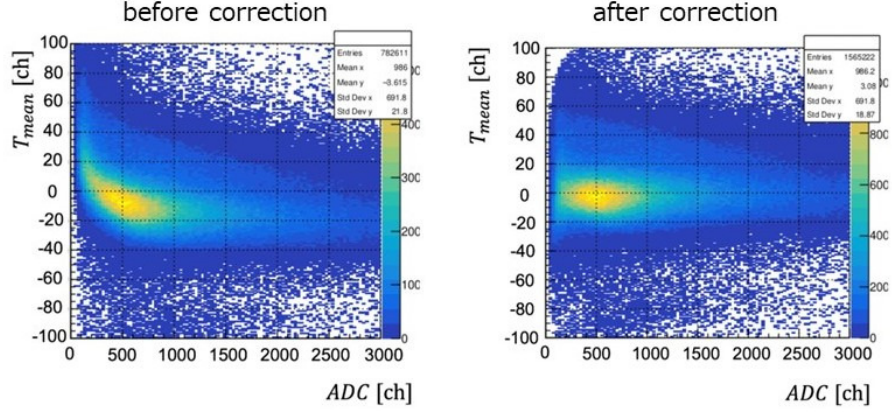


Figure 18: Mean timing ( $T_{mean}$ ) vs. ADC channels of  $B\gamma$  signals before (left) and after (right) the time-walk collection

trajectories. The  $z$ -hit positions were calculated from the ratio of the ADC signals from two PMTs at the upstream and down stream side as  $z_{ADC} = \ln(ADC_{up}/ADC_{dw})/2$ . Figure 19 (left) shows the scatter plot of  $z$  positions determined by the TPC and the  $z$ -positions determined by ADCs of the  $B\gamma$ . There is a strong correlation. From the fitting to this plot, the attenuation length were obtained as Fig. 19 (left). The x axis is the channel from 0 to 47 for the first layer, from 48 to 95 for the second layer and from 96 to 143 for the third layer. The y axis is the attenuation length for each module. The attenuation length is from 560 mm to 815 mm.

The  $z$ -hit positions were calculated from the time difference between two PMTs at the upstream and down stream side. Figure 20 (left) shows the scatter plot of  $z$ -positions determined by the TPC and the  $z$ -positions determined by the time difference of the  $B\gamma$ . There is a strong correlation. From the fitting to this plot, the effective velocities were obtained as Fig. 20 (left). The x axis is the channel from 0 to 47 for the first layer and from 48 to 95 for the second layer. The y axis is the effective velocities. The effective velocity is from 148 mm/ns to 160 mm/ns.

The  $z$ -positions,  $z_{TPC}$ ,  $z_{TDC}$  and  $z_{ADC}$  are determined by the TPC, the  $B\gamma - TDC$ , and  $-ADC$ , respectively. The distributions of these differences between them are fitted by the Gaussian function to obtain the standard deviations of  $\sigma_{TDC-ADC}$ ,  $\sigma_{TDC-TPC}$ , and  $\sigma_{ADC-TPC}$ . From these deviations, each resolutions,  $\sigma_{TPC}$ ,  $\sigma_{TDC}$ , and  $\sigma_{ADC}$ , are calculated to be

$$\sigma_{TPC} \sim 20 \text{ mm} \quad (5)$$

$$\sigma_{TDC} = 49 \sim 76 \text{ mm} \quad (6)$$

$$\sigma_{ADC} = 57 \sim 83 \text{ mm} \quad (7)$$

Figure 21 shows the  $z$ -position resolutions by  $B\gamma$ -ADC (top) and  $-TDC$  (bottom).

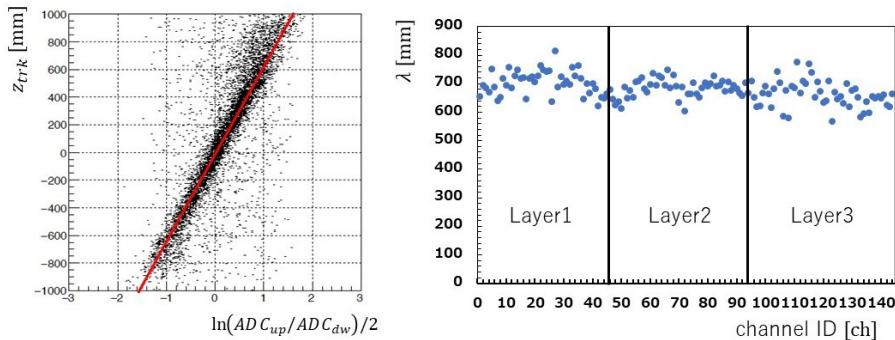


Figure 19: Determination of the attenuation lengths of  $B\gamma$

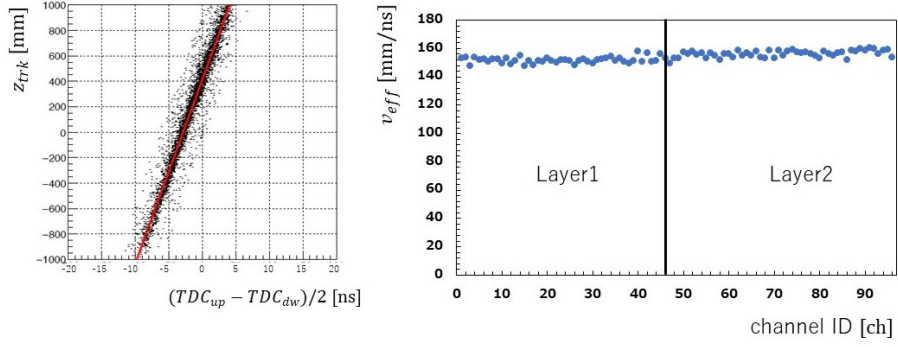


Figure 20: Determination of the effective velocity of the scintillation lights of  $B\gamma$

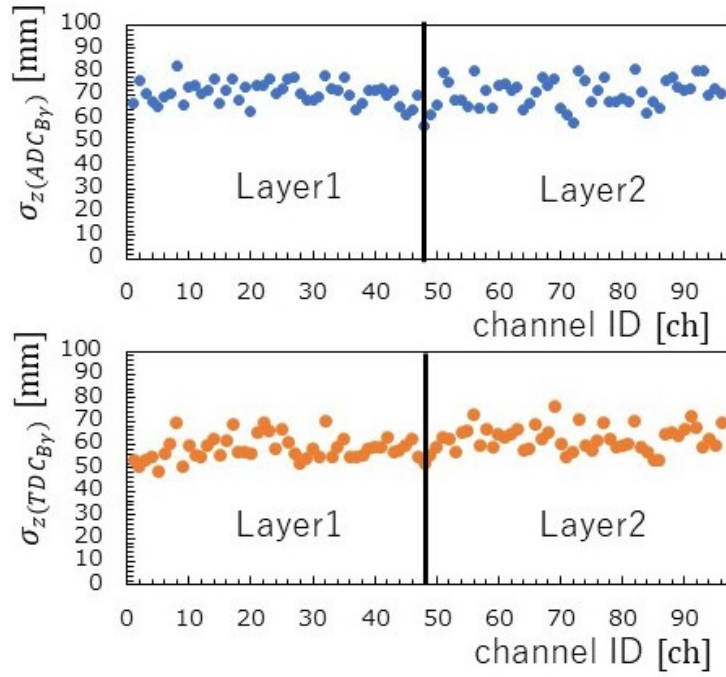


Figure 21: The z-position resolutions of each modules of  $B\gamma$

## 2.7 Neutron counter

(M. Yosoi)

The neutron counter (NC) is a detector to measure neutrons produced by photo-nuclear reactions and emitted forward. It can be used, for example, to search for meson-baryon bound states  $X$  in the reaction of  $\gamma + d \rightarrow n + X$ . Since neutrons have no electric charge, they need to be measured indirectly using charged particles generated in some neutron induced reactions. The most efficient method for high-energy neutrons is to use recoil protons produced by elastic scattering due to the nuclear force with protons in the detector material. For this reason, plastic scintillators, which contain a high amount of hydrogens and can be manufactured inexpensively in large dimensions, are usually used as detectors.

NC for the LEPS2 solenoid experiment has been constructed by rearranging a large number of scintillators used as the range stack in the E949 experiment that were transferred from BNL (Brookhaven National Laboratory, USA) with the large solenoid.

### 2.7.1 Mechanical design

The layout of NC is shown in Fig. 22. NC is a hodoscope with two layers and each layer consists of 24 scintillator blocks, The size of each block is 182 cm long and 76.2 cm thick. There are two kinds of blocks with different width; one with an average width of 127 mm and the other with an average width of 178.5 mm, and both side edges of them have been tapered by  $7.1^\circ$ . As shown in Fig. 22, the narrower blocks are placed near the center and the wider ones at both sides. Each block consists of four scintillator plates stacked on top of the other. Each scintillator is BC-408 with the thickness of 19.05 mm. Two photomultiplier tubes (PMT: EMI-9954B) are attached to each end of the block via light guides.

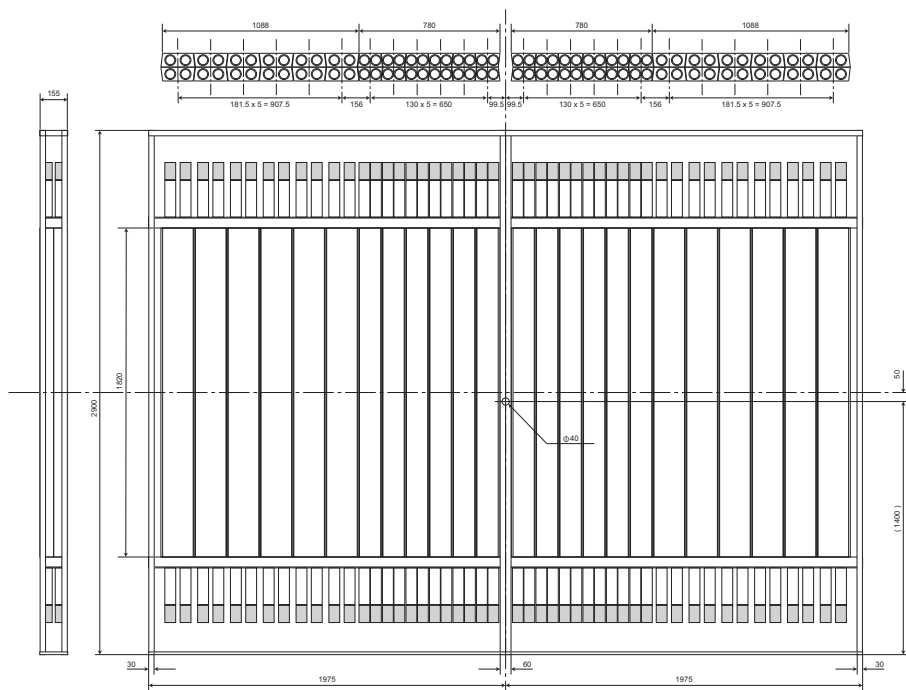


Figure 22: Drawing of the LEPS2 neutron counter (NC).

The overall size of the NC is 3,800 mm (W)  $\times$  1,820 mm (H) and it is placed at the distance of 8 m from the target center. Then, NC covers a solid angle of about 100 msr from the center of the target. However, there is a dead zone of 60 mm width vertically in the center due to the aluminum fixing frame. The photon beam passes through a 40 mm diameter hole in the frame and enters the beam dump downstream. The center of the NC is 45 mm above the beam axis. The detection efficiency of high energy (0.5 GeV – 1 GeV) neutrons incident on the NC is estimated from simulation to be about 20%

for two layers (152.4  $\mu\text{m}$ ) when the lower energy threshold of detection is 1 MeV.

### 2.7.2 Performance study

About half of the scintillator blocks were individually evaluated for their performance with cosmic rays when they were loaned to the KEK Sterile- $\nu$  Group before assembling them. As a result, when the signals from the four PMTs were read out independently, a time resolution of about 190 ps was obtained for the narrower blocks and 260 ps for the wider blocks, respectively. In the LEPS2 experiment, the signals of the two PMTs at each end are summed just after the PMT outputs because of lack of the number of readout circuits as well as the desire to lower the energy threshold as much as possible. Therefore, only two channels of time information are used so that the time resolution is expected to be about  $\sqrt{2}$  times worse than the above. In fact, preliminary analysis of the LEPS2 experiment with a liquid hydrogen (deuterium) target has yielded the time resolution of 250 ps at the center and 300 ps at the edges, respectively, for narrower blocks. Detailed study in NC performance is currently in progress.

## 2.8 Counters for trigger decisions

(M. Niiyama)

In the LEPS2 Solenoid experiment, in addition to the detectors for physics analysis mentioned above, detectors have been prepared to determine the trigger conditions for data acquisition. One is the up counter, and the other is the  $e^+e^-$  counter. The up counter is provided to discriminate events where the beam photons have been converted into electron-positron pairs before reaching the target. It is placed just upstream of the target to detect these electrons and positrons. The up counter has a rectangular shape with dimensions of 20 cm in height and 15 cm in width, and a thickness of 5 mm. Events with the up counter hits are excluded from the data acquisition criteria.

Most of the gamma-ray beam passes through the up counter and is irradiated onto the target. At the target, the generation of electron-positron pairs through electromagnetic interactions occurs with a much higher probability than hadron generation, filling the bandwidth for data collection with these events. Therefore, it is necessary to ensure that these electron-positron pair generation events do not meet the trigger conditions for data collection. The majority of electrons and positrons generated at the target are wrapped around the solenoidal magnetic field and move downstream along the beam axis. The  $e^+e^-$  counter is placed on the beam axis downstream of the drift chambers to detect these electrons and positrons. The  $e^+e^-$  counter has a hexagonal shape with an inscribed circle of 13 cm and a thickness of  $\sim 5$  mm. Events with the  $e^+e^-$  counter hits are excluded from the data acquisition criteria.

## 2.9 Cryogenic target system

(T. Ishikawa and M. Yosoi)

The cryogenic target system used in the LEPS2/Solenoid experiment was originally developed for the LEPS/NTPC experiment at the BL33LEP beamline. The system was also used in the LEPS2/BGOegg experiment, but the geometrical structure around the target cell has been modified. Liquid hydrogen or deuterium is stored in a cryostat, which consists of a refrigerator, a heat transfer pipe connected with a target cell, and a heat radiation shield. The refrigerator is a two-stage Gifford-McMahon (GM) refrigerator, Sumitomo Heavy Industries 4K GM Cryocooler RDK-408D, which is covered with a heat shield made up of copper for preventing from heating by black-body radiation, and vacuum chamber made of stainless steel and carbon fiber reinforced plastics (CFRP). The refrigerator is vertically mounted at approximately 1460-mm upstream of the target center and attached to the heat transfer pipe leading to the target center. The protruding pipe is made of oxygen-free copper, C1020, with a thickness of 4 mm. The length of the pipe is approximately 1420 mm and cell is attached at its end. The pipe is covered with a copper radiation shield with an inner diameter of 71 mm and a thickness of 1 mm except in the cell region. The capsule-shaped cell with a thickness of 148 mm (146.5 mm at normal temperature and pressure) is separated from vacuum with the entrance and exit windows made of polyimide (DuPoint

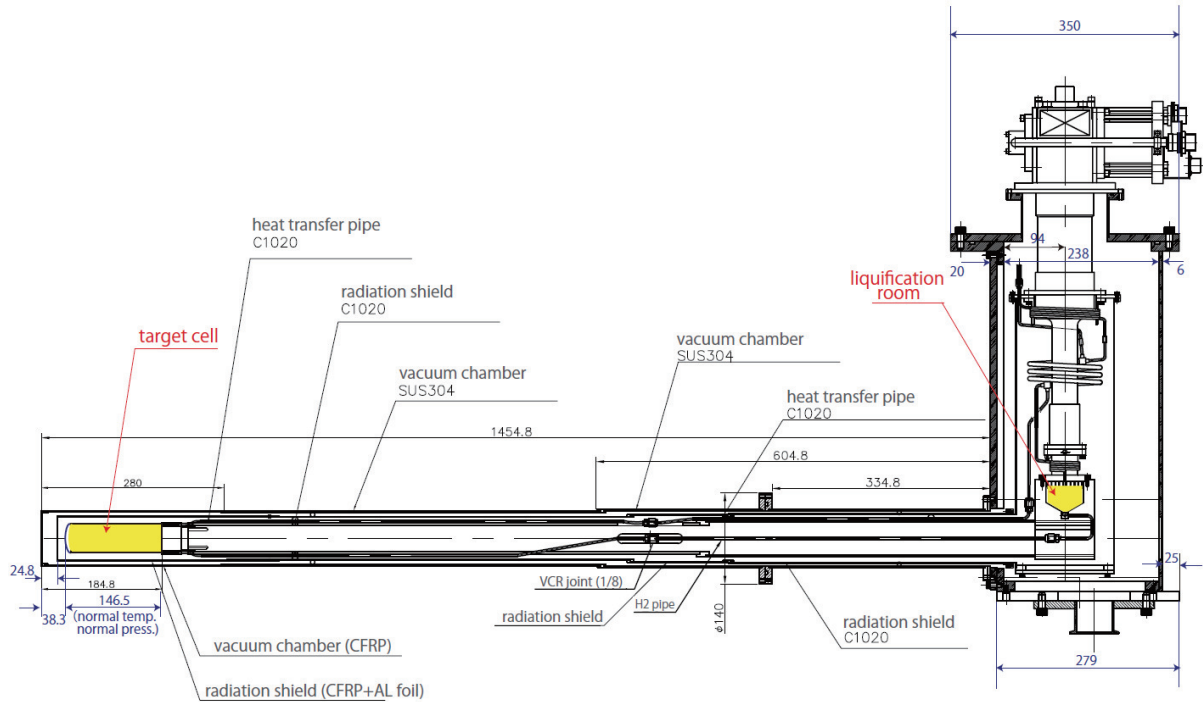


Figure 23: Schematic view of the liquid hydrogen (deuterium) target system.

Kapton) foil with a thickness of  $125 \mu\text{m}$ . The cell is covered with a 1-mm-thick cylinder made of CFRP with an inner diameter of 67 mm wrapped with aluminum foil, and a 1 mm-thick CFRP cylinder with an inner diameter of 82 mm forming a part of the vacuum chamber, the downstream of the protruding vacuum pipe. A hydrogen or deuterium gas is liquified and accumulated in the liquification room right below the refrigerator, and is then directed through pipes to the target cell. The protruding vacuum pipe, connected to the downstream CFRP pipe, is made of 1-mm-thick stainless steel, SUS304. The vacuum chamber also has entrance square window made of Kapton foil with a side of 65 mm. The cryogenic target system is placed so that the center of the target cell is positioned at the designed target center of the Solenoid spectrometer, which is at approximately 680-mm downstream from the front face of the shield yoke of the solenoid magnet. Fig. 23 shows the cross-sectional view of the cryogenic target. It should be noted that the heat transfer pipe is shrunk to keep a cryogenic target by roughly 6 mm from the room temperature.

The target cell is manufactured by bonding a Kapton film to a copper base using a thermally conductive epoxy encapsulant, Henkel Loctite, Stycast. The cell consists of three parts: central cylinder, downstream cap, and upstream window. The cell and liquification chamber are connected with two 1/8-inch pipes: one is for delivery of a liquid target from the lower side of the liquification room to the lower side of the cell and the other is for return of the target from the upper side of the cell to the heat exchanger at the upper side of the chamber. The volumes of the target cell and liquification chamber are approximately 270 cc and 110 cc. When the liquid target is vaporized, more than 300 L of the corresponding gas is produced. We prepare several bottles, so-called the buffer tank, with a total volume of 436 L for hydrogen and 600 L for deuterium. We produced a liquid hydrogen or deuterium target by using the stored gas in the tank instead of using fresh gas in the bottle. The copper pipe with an outer diameter of 3/8 inch is connected between the tank and the port of the top flange of the chamber, from which the gas is lead to liquification room through the heat exchanger. We fill hydrogen or deuterium gas with an inner pressure of 1.7 bar into the target cell and liquification chamber, close the valve in the connecting pipe, and liquify a part of the filled gas by cooling with the refrigerator so that the inner pressure becomes 1 bar for hydrogen and 1.1 bar for deuterium, respectively.

## References

- [1] M. S. Atiya *et al.*, Nucl. Instrum. Meth. A **321**, 129 (1992).
- [2] M. Akatsu *et al.*, Nucl. Instrum. Meth. A **440**, 124 (2000)
- [3] N. Tomida *et al.*, Nucl. Instrum. Methods A 766 (2014) 283–28.
- [4] K. Watanabe *et al.*, Nucl. Instrum. Methods, **A925** (2019) 188–192.
- [5] H. Goto, master thesis at Osaka University (2016).
- [6] Y. Yanai *et al.* Presentation in JPS Meeting at Sendai, Japan on 19th on Mar. in 2016.